TESTS OF THE CBM RICH READOUT AND DAQ PROTOTYPE

J. Adamczewski-Musch[a], P. Akishin[g], K.-H. Becker[b], S. Belogurov[g,e], J. Bendarouach[c], N. Boldyreva[d], C. Deveaux[c], V. Dobyrn[d], M. Dürr[c], J. Eschke[a], J. Förtsch[b], J. Heep[c], C. Höhne[c], K.-H. Kampert[b], A. Khanzadeev[d], L. Kochenda[d,e], J. Kopfer[b,c], P. Kravtsov[d,e], I. Kres[b], S. Lebedev[c,g], E. Lebedeva[c], E. Leonova[d], S. Linev[a], T. Mahmoud[c], J. Michel[f], W. Niebur[a], E. Ovcharenko[g] *, V. Patel[b], C. Pauly[b], D. Pfeifer[b], S. Querchfeld[b], J. Rautenberg[b], S. Reinecke[b], Y. Riabov[d], E. Roshchin[d], V. Samsonov[d,e,h], V. Schetinin[g,i], O. Tarasenkova[d], M. Traxler[a], C. Ugur[a], M. Vznuzdaev[d]

a *GSI Helmholtzzentrum für Schwerionenforschung GmbH, D-64291 Darmstadt, Germany*

b *Department of Physics, University Wuppertal, D-42097 Wuppertal, Germany*

c *Institute of Physics II and Institute of Applied Physics, Justus Liebig University Giessen, D-35392 Giessen, Germany*

d *National Research Centre "Kurchatov Institute" B.P. Konstantinov Petersburg Nuclear Physics Institute, 188300 Gatchina, Russia*

e *National Research Nuclear University MEPhI (Moscow Engineering Physics Institute), 115409 Moscow, Russia*

f *Institut für Kernphysik, Göthe University Frankfurt, D-60438 Frankfurt am Main, Germany*

g *Laboratory of Information Technologies, Joint Institute for Nuclear research (JINR-LIT), 141980 Dubna, Russia*

h *St. Petersburg State Polytechnic University (SPbPU), 195251 St. Petersburg, Russia*

i *Bauman Moscow State Technical University, 105005 Moscow, Russia*

* corresponding author.
E-mail address: eovchar@jinr.ru (E. Ovcharenko)

Abstract

The CBM RICH detector is an integral component of the future CBM experiment at FAIR, providing efficient electron identification and pion suppression necessary for the measurement of rare dileptonic probes in heavy ion collisions. An overview of the CBM RICH readout and DAQ system is given, consisting of the PADIWA preamplifier-discriminator board, the TDC-HUB board TRB v3, and DAQ and analysis code in the CbmRoot framework. The laboratory setup built for studying the timing characteristics of the readout chain and the analysis results obtained using the laboratory measurements are presented. The fine time calibration and inter-channel delay correction techniques and their implementation and effect are discussed.

Introduction

The Compressed Baryonic Matter (CBM) [1] experiment is planned at the future Facility for Antiproton and Ion Research (FAIR) [2] in Darmstadt, Germany. The physics program of CBM is aiming at studying the phase diagram of strongly interacting matter and the equation of state of the baryon matter at very high baryon densities which can be achieved in the collisions of relativistic heavy nuclei in the fixed target experiment.

In order to realize the physics program [3], yields and distributions in the phase space of the particles born in the interaction area should be measured. For that in each event one has to: reconstruct short-lived particles, including extremely rare ones, by measuring their decay products; identify relatively long-lived particles; measure the centrality of events; determine the reaction plane.

The experimental setup is organized as follows. The silicon tracking system (STS), consisting of 8 individual tracking layers of double-sided silicon strip-detectors is located inside a large superconducting dipole magnet. The measurement of di-electron probes requires excellent particle identification, in particular e/π separation, which is achieved using a large Ring-Imaging Cherenkov detector, the CBM RICH. For measurement of di-muon probes, the RICH is interchanged with a large Muon detection system (MUCH). Particle reconstruction and tracking is further extended using a Micro Vertex Detector (MVD), Transition Radiation Detectors (TRD), a Time-of-Flight (ToF) detection system, an Electromagnetic Calorimeter (ECAL), and a Projectile Spectator Detector (PSD).

The CBM experiment is characterized by the high particle multiplicity, high density of tracks at the small polar angle and high primary interaction rate. Due to that the detector systems will have tens of thousands of densely packed readout channels working in self-triggered mode and providing enormous amount of data which needs to be gathered and analyzed “on the fly”.

The above requirements led to the concept of the CBM RICH readout scheme based on the fast multi-anode photomultiplier (MA PMT) Hamamatsu H12700 [4] and time-sensitive electronics. This paper describes the results of the laboratory test of the CBM RICH readout and DAQ system prototype.

1. A 64-channel readout module

The CBM RICH readout and DAQ system is supposed to be composed as follows:

1. readout channels, each including: analog part – a low-pass filter and a pre-amplifier; discriminator with an adjustable threshold which gives a logical LVDS output signal with duration depending on the input signal amplitude; TDCs producing timestamps for the leading and the trailing edges of the logical signal;
2. several levels of data concentrators gathering data from multiple channels;
3. Data Processing Boards (DPB) which perform combining of input data into timeslices and possibly some basic data processing in hardware;
4. FLIB boards which serve as interfaces between the custom electronics and the PC; FLIB stands for FLES Interface Board and FLES [5] for First Level Event Selector – a complex system for online event reconstruction and selection of interesting data.

In the tested prototype the first two items had been realized.

The readout chain starts from the MA PMT detecting single Cherenkov photons. It is characterized in detail in [6]. Its advantages are high photosensitive cross section area (87% packing density), square shape which allows to cover large areas with minimal gaps, low rise time (0.65 ns), low transit time jitter (0.28 ns) and low thermoelectron rate (~50 Hz/channel).

All readout and digitizing electronics of CBM RICH can be grouped into 64-channel modules corresponding to one MA PMT each. Figure 1 shows the scheme of one 64-channel module. It includes 4 PADIWA boards and one TRB v3 board [7].

PADIWA (Figure 2, left) is a 16-channel front-end board [8] developed in the GSI electronics department. Each channel has the signal and the ground input lines, a low-pass filter (~100 MHz), a preamplifier and a discriminator. The input impedance is approx. 100 Ohm. The inputs are located such that the board could be connected to the MA PMT in both possible orientations. After amplification the signal comes into the FPGA. Setting the individual reference voltage for one line of the differential FPGA input, one can provide the discrimination threshold. The output lines and the FPGA configuration lines are coupled in a single socket of 20 LVDS lines. 4 lines are used to configure the FPGA and 16 lines are the output lines.

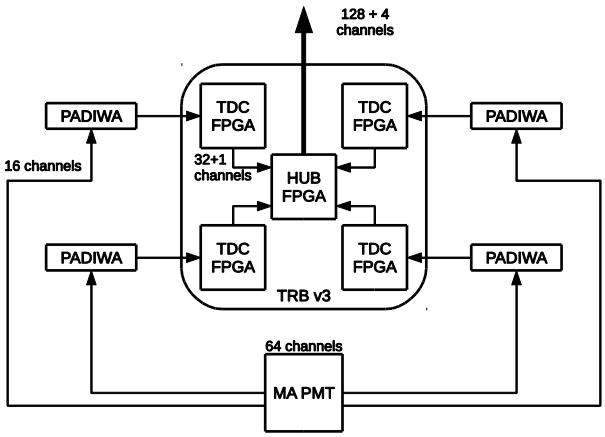

Figure 1. The scheme of one MA PMT readout consisting of 4 PADIWA boards and one TRB v3 board.

TRB v3 (Figure 2, right) is a multifunctional board with 5 FPGAs which can be programmed independently. The TRB v3 configuration used in this work has 4 peripheral FPGAs programmed as TDCs and 1 central FPGA programmed as HUB. A signal from one PADIWA channel is split at the first stage of the TDC FPGA. Then these two identical pulses are processed by two independent TDC channels – one detects the leading edge and the other detects the trailing edge. Thus the time-over-threshold (ToT) can be measured. Each FPGA also has one synchronization channel which gives total 132 output channels of TRB v3. There are special sockets for addon boards next to each FPGA. A dedicated addon board was used to connect the signal flat cables from the PADIWA boards. The TRB v3 board has Ethernet ports for bidirectional communication with other TRB v3 boards or PC using the TrbNet protocol.

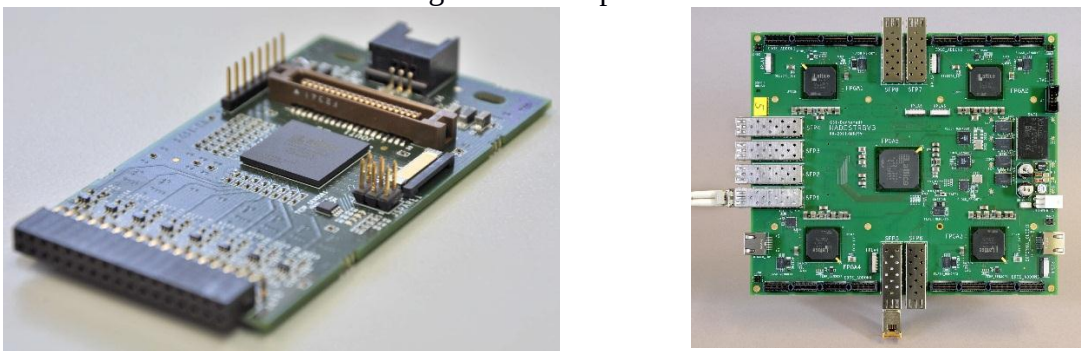

Figure 2. Photos of the PADIWA front-end board (left) and the TRB v3 board (right).

Each peripheral FPGA has inside 32 independent regions with a single TDC channel programmed. These regions are located in different places on the matrix so each TDC channel has different length of the signal path. The even channels are configured to detect the leading edges while the odd channels are configured to detect the trailing edges. The difference in signal propagation between the two TDC channels serving one input channel has to be calibrated using a high-precision generator of square pulses.

The detection of an edge in the TDC is done in two stages [9]. At the first stage the time is registered using a circular counter which is controlled by the clock with 5 ns period. The most significant 28 bits are called epoch and the rest 11 bits are called coarse time. At the second stage the fine time is measured. The time value is coded in two messages – epoch and timestamp. In order to decrease the output data rate the epoch value, which is incremented every 10.24 us, is transmitted once for a group of timestamps belonging to this epoch.

The timestamp contains the coarse time and an additional 10-bits register for the fine time value. The register is filled from the fine time counter implemented using Tapped Delay Line (TDL) on 512 elements. If all delay elements were identical, full time would be $T = \left(Epoch \cdot 2048 + Coarse - (Fine/512)\right) \cdot 5\text{ns}$. However, due to imperfections in the electrical components there are fluctuations in the parameters of the delay line elements; hence, calibration of fine time measurements is required. The calibration procedure and the quality of calibration are discussed in the sections 3.2 and 4.1.

The FPGAs on the TRB v3 board create 4-byte messages of one of several different types. The logic of the messages building is described in detail in the documentation [10].

Every readout channel has some individual delay between the instance of the photoelectron knockout and registered timestamp of the leading edge. This delay is due to the electron avalanche development in the dynode system, signal propagation in the wires and logical elements switch. The procedure of the delay correction is discussed in the section 3.3.

2. Experimental setups

2.1 The laboratory setup for direct TDC measurements

In order to measure the time-over-threshold it is necessary to calibrate the relative delays of TDC channels. The setup shown in the Figure 3 has been used to calibrate the TDCs. The setup consisted of one TRB v3 board with standard firmware (4 TDCs and 1 HUB) with 4 addon LVDS receiver boards installed. In order to imitate the LVDS output of PADIWA the direct and inverted output signals of a high-precision pulser were converted into one LVDS signal. This signal was then split into two and sent to different pairs of input channels using identical cables.

The pulser was set to a square pulse 10 ns long with 1 ns rise and fall time. The synchronization output of the pulser was sent to the readout trigger input of the TRB v3 board after required TTL to LVDS conversions using two auxiliary boards. The readout into PC was performed using standard Ethernet cable directly from the TRB v3 board via the Ethernet switch. This setup also allows to measure the precision of edges' timestamp detection by the TDC only. The results are discussed in the section 4.2.

2.2 The laboratory setup for tests of the 64-channel readout module

The laboratory setup implements the 64-channel readout module described in the section 1. It was located in the dark room and constructed inside the light-tight box. A laser Alphalas Picopower LD405 coupled with the pulser Alphalas PLDD-250 [11] was used as the source of light. Duration of the light pulse is ~40 ps. The light of the laser was transported into the box using the optical fiber. In order to provide most homogeneous illumination of the MA PMT the light was diffused with a special matte glass.

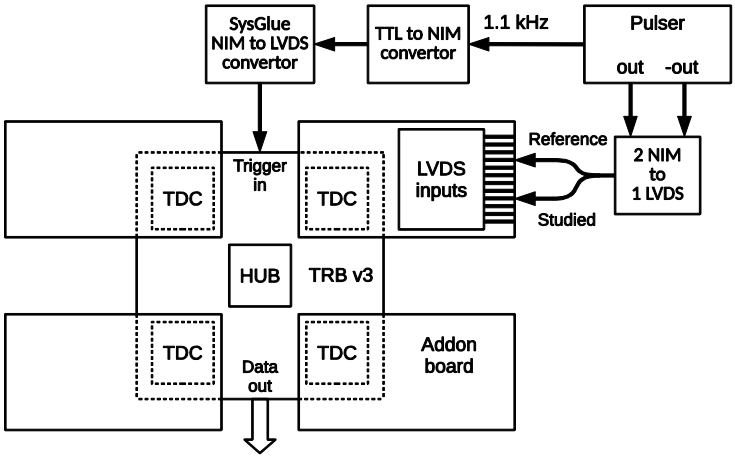

Figure 3. Scheme of the laboratory setup for direct TDC measurements.

The MA PMT was located at the distance of about 30 cm from the diffusing glass. The MA PMT was isolated from eventual external light with a printed plastic tube. The PMT was kept in darkness for about 1 hour before measurements. To eliminate the pick up from the luminescent lamps the light was switched off even in the control room.

The laser intensity was set such that the MA PMT channels worked in the single photoelectron regime. The registration rate in each channel was about 10% of the laser frequency.

The specially designed carrier-board holds the MA PMT and the front-end boards. It connects the MA PMT anodes to the corresponding PADIWA inputs, provides light insulation and high voltage distribution. The outputs of the PADIWA are connected to the TRB v3 inputs via 2 meter-long flat cables consisting of 20 twisted pairs each.

The readout and DAQ system is self-triggered i.e. every pulse in the input channel is digitized if it rises above the discrimination threshold and the timestamp is pushed into the readout buffer. The trigger output of the pulser controlling the laser has been also used to flush the readout buffer into the PC. The readout trigger pulses are digitized the same way as normal signal and pushed in the output data stream. This allows to analyze the detected timestamps with regard to the laser flashes.

3. Software

The software for the CBM RICH data processing is implemented in the CbmRoot framework [12]. All stages from readout to analysis can be performed «on the fly» without recording any intermediate information on the disk. The data processing pipeline includes the following stages: unpacking, calibration, hit building, event building, reconstruction and analysis. The last two are relevant for the Cherenkov rings and are not discussed here. Functionality and implementation of all the other blocks is described below. In the present work the DABC [13] software has been used as an interface between the hardware and the CbmRoot. The dedicated code for the timing characteristics analysis has been implemented in the CbmRoot framework.

3.1 Unpacking

Unpacking is the first stage of processing of the data received from the electronics, in our case in the HLD file format [14]. There is possibility to process data coming both from the detector («online») and data stored in the file («offline»). Unpacking procedure is implemented in the task-class *CbmRichTrbUnpack*. A special ROOT array of identical objects implemented using *TClonesArray* class is filled on each iteration with *CbmTrbRawMessage* objects.

3.2 Fine time calibration

The fine time calibration procedure is typical for the digital delay line realized using Tapped Delay Line (TDL) technology [15]. It is based on the fact that the distribution of time stamps from a source uncorrelated with the FPGA clock has to be uniform. Deviations from this uniformity stem from varying bin sizes of the TDC due to fluctuations of the technology and can be corrected. As result of analysis of some portion of data a discrete calibration function $f_{calib}(Fine)$ is built for each channel. This function gives the correspondence between the fine time counter value and time in nanoseconds. The full time is computed using the following formula:

$T = Epoch \cdot 2048 \cdot 5ns + Coarse \cdot 5ns - f_{calib}(Fine)$.

The fine time calibration procedure is implemented in the singleton-class *CbmTrbCalibrator*, which is not a part of the pipeline but can be called from any stage of data processing. The table can be saved in the file and used in repeated analysis runs.

3.3 Inter-channel delay calibration

To compensate the spread of signal propagation time in different channels the delay calibration tables can be built basing on the result of the first run of data analysis using the «*ExtractDelays*» and the «*BuildDeltaTable*» macros of CbmRoot. The possibility to import these tables is implemented in the *CbmTrbCalibrator* class.

The algorithm of building the corrections table is as follows. Let the pixels of the photosensitive camera composed of N photomultipliers be enumerated from 1 to $64 \cdot N$. The leading edges with timestamps inside a certain time window around the trigger signal (laser) are selected for analysis. The width and the position of the window have to be set by the user. In our case the window spanned from -20 ns to 80 ns.

The differences of leading edges' timestamps for every pair of channels are histogrammed using all the bulk of the selected data. The mean value or the position of the maximum of the distribution can be used as the measure of the delay. The obtained values fill the $N \times N$ skew-symmetric matrix. Afterwards the user may choose the reference channel to build the correction table which actually is one column of the matrix.

3.4 Hit building – edge matching

Every detected photon produces two messages with timestamps of leading and trailing edges respectively. The edge matching algorithm has been implemented in the task-class *CbmTrbEdgeMatcher* which stands in the pipeline after the unpacking stage and takes calibrated timestamps as input. There is a buffer for each channel which is filled with the leading edges as they come. Then, when a trailing edge comes, the corresponding buffer is searched for the leading edge closest in time. Figure 4 shows an example of the leading edge buffer with a few candidates of leading edges for the trailing edge being processed. The matched pair of edges forms a hit. Time-over-threshold (ToT), i.e. time difference between the leading and trailing edges, is the hit parameter.

Figure 4. Input information for the task of finding the corresponding leading edge.

The buffer has to be flushed periodically to avoid overflow because of the occasional single edges without a pair. The number of unpaired edges has strong dependence on the load of the TDC input bus which in turn depends on the discriminator threshold.

3.5 Event building

The data pushed by the digitizing and data concentrating electronics (TRB v3) come into software in portions called DAQ-event. The procedure of reconstruction of «real» events is required to provide correct information for the next stages – reconstruction and analysis. The event building procedure is illustrated by the Figure 5.

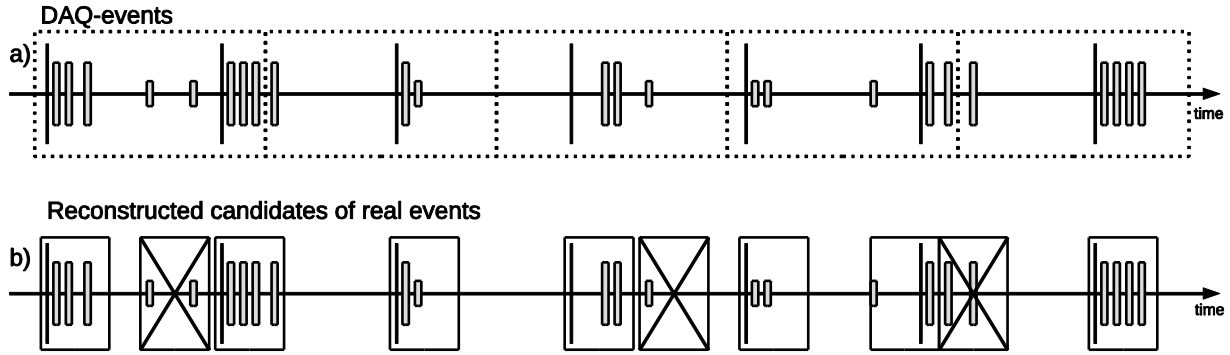

Figure 5. The idea of event building: (a) input data gathered in DAQ-events (dotted boxes); (b) reconstructed candidates of real events; the crossed boxes correspond to rejected event candidates containing no trigger. Thin long lines – trigger signals (laser), mid-length rectangles – signal, coming from light, short rectangles – noise signals.

The real event may fall onto the boundary of the DAQ-events, besides, the input messages not necessarily come ordered in time, for these reasons several DAQ-events must be under consideration when building a real event. Thus first clusters of hits in time need to be found in a rather wide interval of time – potential event – then real events containing a laser flash have to be filtered using some criterion, i.e. presence of a trigger message of a certain type.

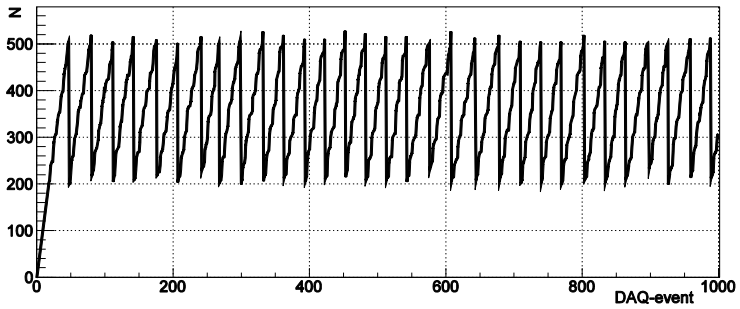

Figure 6. Diagram of the number of found events in the buffer vs. number of the processed input DAQ-event. The minimum and the maximum levels set are 200 and 500 accordingly.

The described algorithm is implemented using a buffer of hits. As the input messages are being unpacked they are pushed into the buffer. On each iteration recognition of event candidates is performed and their number N is determined. To avoid memory overflow, it is controlled by two adjustable levels – minimum and maximum ones. When N reaches the minimum level pushing of output event candidate is performed along with getting one input DAQ-event. When N crosses the maximum level, the recognized event candidates are flushed FIFO to the minimum level. Figure

6 shows the part of the diagram of the number of events found in the buffer vs. number of the input DAQ-event processed.

4. Results

4.1 Fine time calibration

An example of the calibration function is shown in the Figure 7 (left). The function can be fitted by the linear function which is unambiguously defined by two values of the fine time counter, corresponding to the fine time of 0 ns and 5 ns respectively. Non-linearity and stability of the calibration function is discussed elsewhere [16]. The values defining the linear approximation of the calibration functions for all the channels are plotted in the Figure 7 (right). Though the distribution occupies two separate domains, it is rather compact. The solid square indicates the parameters of the averaged linear function. Depending on the specific measurement task, either individual or averaged linear function can be used instead of the exact calibration function. The effects of such a substitution are discussed in the next section.

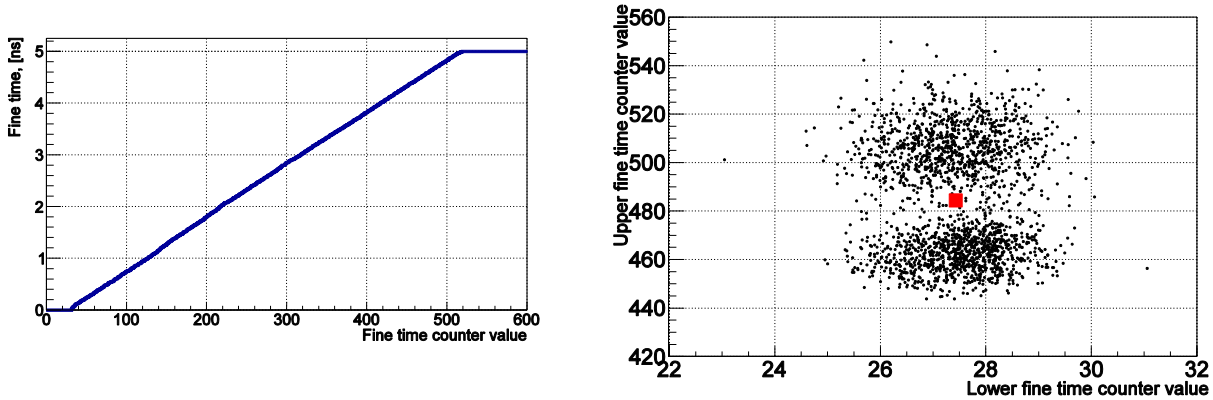

Figure 7. An example of the calibration table shown as a graph (left) and the distribution of the calibration function linear fit parameters (right).

4.2 Direct TDC measurements

The differences of the leading edges' timestamps in all possible pairs of channels as well as the measured pulse width (ToT) in each channel have been histogrammed before and after the fine time calibration, see an example in Figure 8 (a,b,c,d). The mean values of the differences are not equal to zero, and the measured pulse widths are not equal to 10 ns. It indicates that the correction of inter-channel delays is necessary. The pulse widths distributions obtained in such measurements have been used to build the table of trailing edge delay corrections. The effects of linear fit substitute for the calibration function can be seen in Figure 8 (e,f) where the individual and averaged linear fits are used.

The usage of the exact calibration function is required to achieve the best possible time precision of the TDC. The width of the distribution of the leading edges timestamps in two TDC channels, which fluctuate independently, is 30 ps (FWHM), which corresponds to 21 ps time precision. Usage of the individual linear fit results in increase of the FWHM to 70 ps and usage of the averaged linear function gives upto 90 ps (FWHM) in the worst channels (time precision 50 ps and 64 ps correspondingly). The usage of the averaged linear function for calibration results in not having the double-peak distribution, typical for the case without fine time calibration, but in some cases this leads to increase of the width of the distribution.

If it is impossible to perform the full fine time calibration, for example due to the small amount of the input data, not sufficient to produce the calibration functions, one can use the averaged calibration function. In particular in the case of CBM RICH the time precision is of the order of a

few hundred picoseconds, so the averaged fine time calibration can be used without noticeable effect.

4.3 Inter-channel delay and the time precision of the readout channel

The differences of the leading edges' timestamps in all possible pairs of channels fired in the given laser event were histogrammed. A typical distribution is shown in the Figure 9 (left). Along with such regular distributions, distorted time spectra containing one or two additional peaks have been observer. For getting the best results, only channels producing the distorted peaks in minimum number of pairs can be taken as reference. The FWHM of a regular distribution is roughly $\sqrt{2}$ times bigger than the time precision because both timestamps fluctuate independently. It gives the time precision of 0.57 ns for the example shown in the Figure 9 (left). This number exceeds the MA PMT transition time jitter and is dominated by the walk of the leading edge of the logical signal due to fluctuations of the single photoelectron amplitude. The walk corrections can be introduced if ToT is correctly measured. That's not a case in this study, see the section 4.4. On the other hand, the achieved value of the time precision is sufficient for the CBM RICH operation.

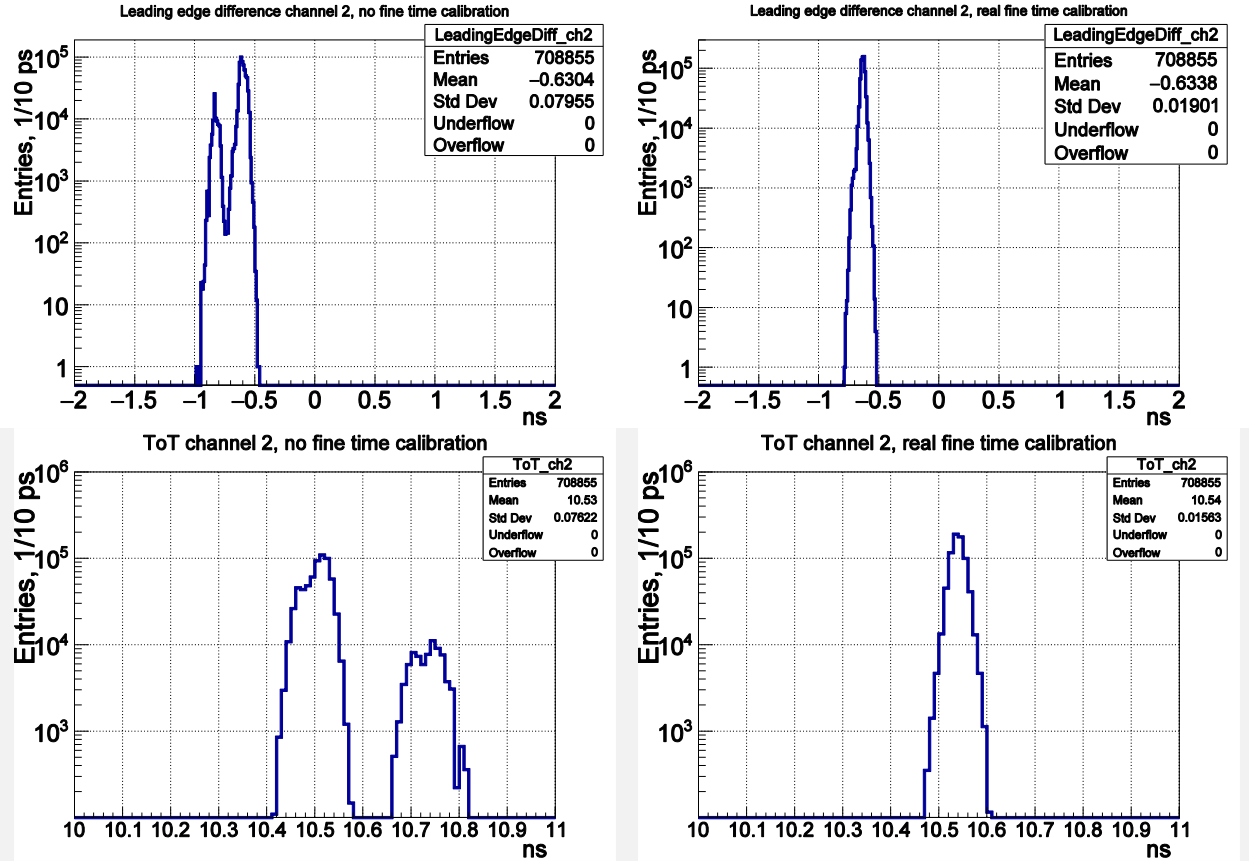

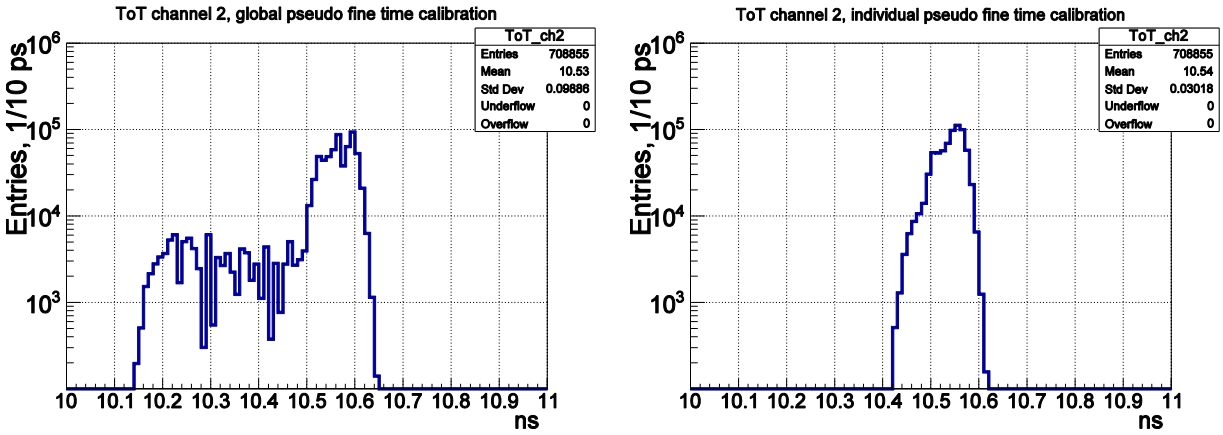

Figure 8. Fine time (FT) calibration effect demonstrated using the direct TDC measurements results; difference between the leading edges of a single 10 ns-wide pulse detected by two TDC channels: (a) without FT calib., (b) with FT calib. using exact table, (c-f) the measured pulse width by one of the two studied channels: (c) without FT calib., (d) with FT calib. using exact table, (e) with FT calib. using averaged linear function, (f) with FT calib. using approximated linear function.

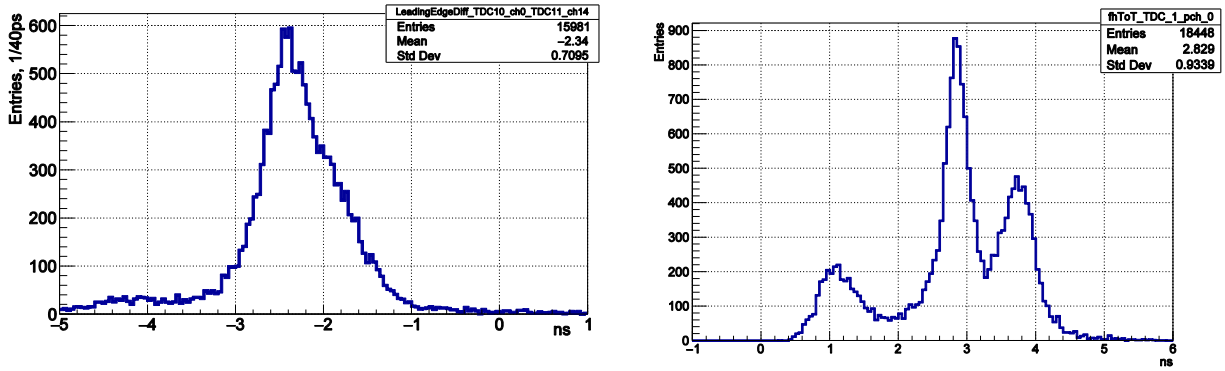

Figure 9. The typical «leading edge difference» distribution (left, the FWHM is approx. 800 ps) and the typical ToT distribution (right). The left distribution is shown with fine time calibration applied, its mean value (-2.34 ns) is taken as the inter-channel delay correction for this pair of channels.

4.4 Time-over-threshold

The typical ToT distribution measured with the laser in the lab setup is shown in the Figure 9 (right). In contrary to what is expected it contains several peaks. Such peaks are likely due to the periodic pickup in the line between the discriminator and the TDC, see e.g. [17]. The ToT can be used in the RICH DAQ system for improving the time precision by implementing the walk correction and for improving separation of the single electron signals from the noise. Fortunately, both issues seem not to be of a crucial importance for the CBM RICH. Nevertheless, placing the discriminator and the TDC on the same board and careful circuitry should help to improve the performance. The recently developed front-end board, called DIRICH [18] and considered as the next generation prototype, may solve the problem.

Conclusions

The prototype of the CBM RICH readout and DAQ system has been assembled and tested in the lab. It includes one 64-channel module which will be a building block for the entire system. The data processing software including unpacking, calibration, hit building, event building,

reconstruction and analysis modules has been developed and used for studying the performance of the prototype. The fine time calibration and delay corrections have been implemented and applied to real data. The time precision of a single channel without walk correction was found out to be 570 ps FWHM. The time-over-threshold spectra have been built and manifested multi-peak structure likely connected to the periodic noise.

References

[1] Official FAIR site, http://fair-center.eu/

[2] Official CBM site, http://www.fair-center.eu/for-users/experiments/cbm.html

[3] The CBM physics book: Compressed baryonic matter in laboratory experiments B. Friman et. al., Lect.Notes Phys. 814 (2011) pp.1-980

[4] The Hamamatsu H12700 series datasheet, https://www.hamamatsu.com/resources/pdf/etd/H12700_TPMH1348E.pdf

[5] A First-level Event Selector for the CBM Experiment at FAIR, J. de Cuveland, *V. Lindenstruth (for the CBM Collaboration)* 2011 *J. Phys.: Conf. Ser.* **331** 022006

[6] Characterization of the Hamamatsu H12700A-03 and R12699-03 multi-anode photomultiplier tubes, M. Calvi et. al., JINST 10 (2015) no.09, P09021

[7] Official site of the TRB project, http://trb.gsi.de/

[8] TRB3: a 264 channel high precision TDC platform and its applications, A. Neiser et. al. 2013 *JINST* **8** C12043

[9] 264 Channel TDC Platform Applying 65 Channel High Precision (7.2 ps RMS) FPGA Based TDCs, C. Ugur et. al., 10.1109/NoMeTDC.2013.6658234

[10] TRB v3 documentation, http://jspc29.x-matter.uni-frankfurt.de/docu/trb3docu.pdf

[11] Laser and pulser official site, http://www.alphalas.com/products/lasers/picosecond-pulse-diode-lasers-with-driver-picopower-ld-series.html

[12] M. Al-Turany, D. Bertini, and I. Koenig. CbmRoot: Simulation and analysis framework for CBM experiment. In S. Banerjee, editor, Computing in High Energy and Nuclear Physics (CHEP-2006), volume 1 of MACMILLAN Advanced Research Series, pages 170–171. MACMILLAN India, 2006.

[13] Data acquisition and online monitoring software for CBM test beams, J. Adamczewski-Musch, N. Kurz, S. Linev, and P. Zumbruch, 2012 *J. Phys.: Conf. Ser.* **396** 012001

[14] HADES trbnet data formats for DABC and Go4, J. Adamczewski-Musch, S. Linev, E.Ovcharenko, and C.Ugur, GSI SCIENTIFIC REPORT 2012, p. 297

[15] R. Szplet, J. Kalisz, and R. Pelka. Nonlinearity correction of the integrated time-to-digital converter with direct coding. IEEE Transactions on Instrumentation and Measurement, 46:449–453, April 1997.

[16] Development of the CBM RICH readout electronics and DAQ, J. Adamczewski-Musch, et. al., NIM A (2017), 10.1016/j.nima.2017.03.043

[17] Time over threshold in the presence of noise, F. Gonnella, V. Kozhuharov, and M. Raggi, NIM A, Volume 791, 11 August 2015, Pages 16–21

[18] The CBM RICH project, J. Adamczewski-Musch, et. al., NIM A (2016), 10.1016/j.nima.2016.05.102